ICASSP 2024 - 2024 IEEE International Conference on Acoustics, Speech and Signal Processing (ICASSP) | 979-8-3503-4485-1/24/$31.00 ©2024 IEEE | DOI: 10.1109/ICASSP48485.2024.10445930

COUPLED BLOCK-TERM TENSOR DECOMPOSITION FOR NEAR-FIELD LOCALIZATION IN MULTI-STATIC MIMO RADAR SYSTEMS

Liana Khamidullina* *and Martin Haardt**

* Communication Research Laboratory, Technische Universität Ilmenau, Ilmenau, Germany

ABSTRACT

This paper presents a high-resolution coupled rank-$(L_r, L_r, 1)$ block-term decomposition-based near-field localization scheme for multi-static MIMO radar systems. The proposed COBRAS (COupled Block-term decomposition for multi-static RAdar Systems) algorithm uses the exact wavefront model to estimate the target location parameters in 3D space and can be applied to arbitrary array geometries. Compared to the far-field models, the exact near-field wavefront model allows exploiting the distance information for high-accuracy positioning. Moreover, we consider a system with massive antenna arrays, which increases the Fresnel region and expands the range of the near-field assumption. The COBRAS algorithm includes the initial tensor decomposition of the data and further post-processing steps that allow extracting the location parameters. Additionally, we compare the performance of different rank-$(L_r, L_r, 1)$ block-term decomposition algorithms and demonstrate how the employment of coupling improves the localization performance compared to the non-coupled solutions.

***Index Terms*—** Near-field, spherical wavefront, MIMO radar, block-term decomposition, data fusion.

1. INTRODUCTION

The near-field region provides new opportunities and challenges for communication and sensing applications. Compared to the far-field design, the near-field allows exploiting the distance information. Therefore, near-field beamforming can yield a higher spatial multiplexing gain by transmitting different data to users located at different locations in the same direction. Moreover, the near-field is highly beneficial in radar systems: in contrast to far-field systems, it allows a more accurate localization with not only angle but also distance parameters. Until recently, most applications of wireless systems have focused on the far-field assumption. However, operations in the mmWave and THz bands, the use of large antenna arrays, and the deployment of reconfigurable intelligent surfaces make the exploitation of the near-field essential and inevitable [1]: the near-field region increases, and the wavefronts cannot be considered as planar anymore.

Commonly, publications that focus on near-field signal processing consider the Fresnel approximation of the spherical wavefronts [2–6], which uses a Taylor expansion of the true phase distribution of the wavefront across antennas. Alternatively, some authors [4, 7–9] avoid using the Fresnel approximation and utilize the exact spherical wavefront model, which avoids systematic errors introduced by the Fresnel approximation and improves the estimation accuracy. Other tools that demonstrate promising results in the area of multiple-input multiple-output (MIMO) radar signal processing include tensor decompositions and multidimensional signal processing. For example, a canonical polyadic (CP) decomposition-based localization and channel estimation algorithm for massive antenna arrays is proposed in [9]. The authors in [4, 7, 8] employ the CP decomposition for parameter estimation in bistatic MIMO radar systems. The multi-static MIMO radar scenario is considered in [10, 11]. The authors propose to use the coupled CP and coupled rank-$(L_r, L_r, 1)$ decompositions to localize the targets in the far-field. However, the algorithm suggested in [10] is limited to 2D space localization when considering a uniform rectangular array (URA) antenna configuration due to the chosen wavefront model. Tensor-based techniques are also widely employed for direction-of-arrival estimation using a planar wavefront model [12–16].

This contribution focuses on multi-static MIMO radar systems with multiple receiving and transmitting massive antenna arrays. We consider the parameter estimation of multiple targets in 3D space using the exact spherical wavefront model. Moreover, we use the signal model from [10] to arrange the received data as a low-rank tensor and employ a robust coupled block-term decomposition (BTD) algorithm that we presented in [17] to estimate the steering matrices. We also develop appropriate post-processing steps, such as phase unwrapping, the solution of the system of linear equations, and the parameter extraction to obtain the final parameter estimates. We refer to the proposed algorithm as "COBRAS" (COupled Block-term decomposition for multi-static RAdar Systems). In contrast to the algorithm in [10], our approach is designed for near-field systems and uses the exact spherical wavefront model. Additionally, we compare the performance of the different BTD algorithms in terms of their impact on localization accuracy.

Notation. Matrices and vectors are denoted by upper-case ($\boldsymbol{A}$) and lower-case ($\boldsymbol{a}$) bold-faced letters, respectively. Bold-faced calligraphic letters denote tensors ($\boldsymbol{\mathcal{A}}$). The superscripts $\{\cdot\}^{\mathrm{T}}$ and $\{\cdot\}^{\mathrm{H}}$ denote the transpose and Hermitian transpose, respectively. Moreover, we use $\circ$ to denote the outer product.

2. SYSTEM MODEL

We consider a multi-static multi-pulse MIMO radar system that uses M_{T} transmit and M_{R} receive arrays to localize R targets. Each transmitter emits temporally orthogonal signals that impinge on the targets, and their reflections are intercepted by receiving arrays. At the receiver side, the signals are matched-filtered using the known waveforms from the transmitter side. The targets are assumed to be in the near-field region of both arrays, such that the wavefronts of the impinging and reflecting waves can be considered spherical, and the target radar cross section (RCS) is assumed to be uncorrelated from pulse to pulse (Swerling 2 model [18]). In the sequel, we focus on uniform rectangular arrays and describe a high-resolution algorithm to estimate the range, azimuth, and elevation parameters of the dominant wavefronts in 3D space. However, the COBRAS algorithm is also applicable to arrays of arbitrary (known) geometries.

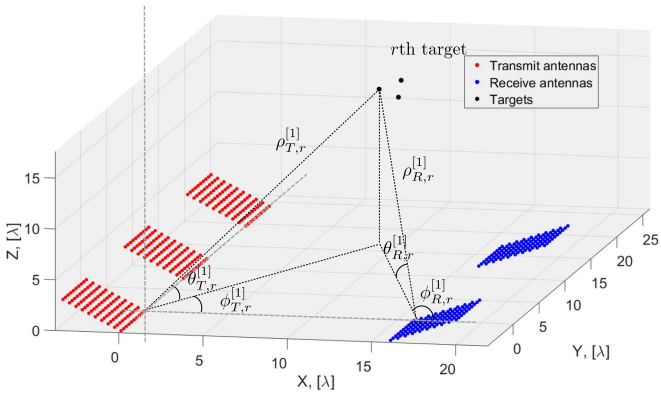

Fig. 1: Scenario geometry with $R = 3$ targets, $M_{\mathrm{T}} = 3$, and $M_{\mathrm{R}} = 2$ URAs. The parameters of one of the targets are given w.r.t. the transmit and receive reference antennas of the 1st transmit and the 1st receive arrays.

2.1. Scenario

An example scenario is shown in Fig. 1. The antennas in the transmit and receive arrays are depicted with red and blue dots, respectively. The black dots denote targets. Each transmit and receive array consists of $N_{\mathrm{T}}^{[m_{\mathrm{T}}]}$, $m_{\mathrm{T}} \in \{1, \ldots, M_{\mathrm{T}}\}$ and $N_{\mathrm{R}}^{[m_{\mathrm{R}}]}$, $m_{\mathrm{R}} \in \{1, \ldots, M_{\mathrm{R}}\}$ antennas, respectively. In the following, to ease the notation, we skip the superscripts $[m_{\mathrm{T}}]$ and $[m_{\mathrm{R}}]$ in the notations of N_{T} and N_{R}, and assume an equal number of antennas in all transmit and all receive arrays. However, the algorithm supports scenarios with different numbers of elements in the antenna arrays. We denote the Cartesian coordinates of the transmit antennas as $\left\{x_{\mathrm{T},n_T}^{[m_{\mathrm{T}}]}, y_{\mathrm{T},n_T}^{[m_{\mathrm{T}}]}, z_{\mathrm{T},n_T}^{[m_{\mathrm{T}}]}\right\}$, $n_{\mathrm{T}} \in \{1, \ldots, N_{\mathrm{T}}\}$ and the Cartesian coordinates of the receive antennas as $\left\{x_{\mathrm{R},n_R}^{[m_{\mathrm{R}}]}, y_{\mathrm{R},n_R}^{[m_{\mathrm{R}}]}, z_{\mathrm{R},n_R}^{[m_{\mathrm{R}}]}\right\}$, $n_{\mathrm{R}} \in \{1, \ldots, N_{\mathrm{R}}\}$.

Every rth target in 3D space is characterized by a set of parameters $\boldsymbol{\Theta}_{\mathrm{T},r}^{[m_{\mathrm{T}}]} = \left\{\rho_{\mathrm{T},r}^{[m_{\mathrm{T}}]}, \phi_{\mathrm{T},r}^{[m_{\mathrm{T}}]}, \theta_{\mathrm{T},r}^{[m_{\mathrm{T}}]}\right\}$ and $\boldsymbol{\Theta}_{\mathrm{R},r}^{[m_{\mathrm{R}}]} = \left\{\rho_{\mathrm{R},r}^{[m_{\mathrm{R}}]}, \phi_{\mathrm{R},r}^{[m_{\mathrm{R}}]}, \theta_{\mathrm{R},r}^{[m_{\mathrm{R}}]}\right\}$, $r \in \{1, \ldots, R\}$, where $\rho_{\mathrm{T},r}^{[m_{\mathrm{T}}]}$ and $\rho_{\mathrm{R},r}^{[m_{\mathrm{R}}]}$ are the distances from the rth target to the reference transmit and receive antennas of the transmit and receive arrays, respectively. Moreover, $\phi_{\mathrm{T},r}^{[m_{\mathrm{T}}]}$ and $\phi_{\mathrm{R},r}^{[m_{\mathrm{R}}]}$ are the azimuth, and $\theta_{\mathrm{T},r}^{[m_{\mathrm{T}}]}$ and $\theta_{\mathrm{R},r}^{[m_{\mathrm{R}}]}$ are the elevation angles, defined with respect to the transmit and the receive systems of coordinates. We assume that the reference antennas of the transmit and receive arrays are located at the origin of the "local" system of coordinates (at every array). Furthermore, we introduce a "global" system of coordinates with the origin at the reference antenna of the first transmit array. Then the coordinates $\{x_{\mathrm{T},m_{\mathrm{T}}}, y_{\mathrm{T},m_{\mathrm{T}}}, z_{\mathrm{T},m_{\mathrm{T}}}\}$ and $\{x_{\mathrm{R},m_{\mathrm{R}}}, y_{\mathrm{R},m_{\mathrm{R}}}, z_{\mathrm{R},m_{\mathrm{R}}}\}$ denote the locations of the m_{T}th and m_{R}th reference antennas with respect to the global origin. Additionally, we introduce a set of Cartesian coordinates of the rth target as $\boldsymbol{\Theta}_{\mathrm{T},r}^{[m_{\mathrm{T}}]} = \left\{x_{\mathrm{T},r}^{[m_{\mathrm{T}}]}, y_{\mathrm{T},r}^{[m_{\mathrm{T}}]}, z_{\mathrm{T},r}^{[m_{\mathrm{T}}]}\right\}$ and $\boldsymbol{\Theta}_{\mathrm{R},r}^{[m_{\mathrm{R}}]} = \left\{x_{\mathrm{R},r}^{[m_{\mathrm{R}}]}, y_{\mathrm{R},r}^{[m_{\mathrm{R}}]}, z_{\mathrm{R},r}^{[m_{\mathrm{R}}]}\right\}$ defined with respect to the reference antennas at the transmit and receive arrays, respectively.

2.2. Signal Model

The received signal $\boldsymbol{Y}_p^{[m_{\mathrm{R}}]} \in \mathbb{C}^{N_{\mathrm{R}} \times T}$ at the m_{R}th receiving array in the pth pulse can be written as [10]

$$\boldsymbol{Y}_p^{[m_{\mathrm{R}}]} = \sum_{m_{\mathrm{T}}=1}^{M_{\mathrm{T}}} \sum_{r=1}^{R} \alpha_r^{[m_{\mathrm{R}}]} \varrho_{r,p}^{[m_R, m_T]} \boldsymbol{b}_r^{[m_{\mathrm{R}}]} \boldsymbol{a}_r^{[m_{\mathrm{T}}]\mathrm{T}} \boldsymbol{S}^{[m_{\mathrm{T}}]\mathrm{T}} + \boldsymbol{N}_p^{[m_{\mathrm{R}}]}, \tag{2}$$

where m_{T}, m_{R}, r, and p are the transmit array, the receive array, the target, and the pulse indices. The complex gain parameters $\alpha_r^{[m_{\mathrm{R}}]}$ represent such effects as attenuation and random phase shifts. The complex quantity $\varrho_{r,p}^{[m_R, m_T]}$ is the reflection coefficient of the rth target relative to the m_{R}th receive and m_{T}th transmit array in the pth pulse. The matrix $\boldsymbol{S}^{[m_{\mathrm{T}}]} \in \mathbb{C}^{T \times N_{\mathrm{T}}}$ contains the transmitted signal during one pulse period after matched-filtering at the receiver, where T is the number of time snapshots in each pulse. The matrix $\boldsymbol{N}_p^{[m_{\mathrm{R}}]} \in \mathbb{C}^{N_{\mathrm{R}} \times T}$ represents the independently and identically distributed (i.i.d.) zero mean spatially and temporally white additive noise with variance σ_n^2. Moreover, the transmit and receive array steering vectors for the rth target are defined in terms of the path differences as $\boldsymbol{a}_r^{[m_{\mathrm{T}}]} = \left[\, 1, \quad \mathrm{e}^{-j\frac{2\pi}{\lambda}\delta_{\mathrm{T},r,2}^{[m_{\mathrm{T}}]}}, \quad \ldots, \quad \mathrm{e}^{-j\frac{2\pi}{\lambda}\delta_{\mathrm{T},r,N_{\mathrm{T}}}^{[m_{\mathrm{T}}]}} \,\right]^{\mathrm{T}} \in \mathbb{C}^{N_{\mathrm{T}}}$ and $\boldsymbol{b}_r^{[m_{\mathrm{R}}]} = \left[\, 1, \quad , \mathrm{e}^{-j\frac{2\pi}{\lambda}\delta_{\mathrm{R},r,2}^{[m_{\mathrm{R}}]}}, \quad \ldots, \quad \mathrm{e}^{-j\frac{2\pi}{\lambda}\delta_{\mathrm{R},r,N_{\mathrm{R}}}^{[m_{\mathrm{R}}]}} \,\right]^{\mathrm{T}} \in \mathbb{C}^{N_{\mathrm{R}}}$, respectively.

The exact expression for the geometric path differences $\delta_{\mathrm{T},r,n_{\mathrm{T}}}^{[m_{\mathrm{T}}]}$ and $\delta_{\mathrm{R},r,n_{\mathrm{R}}}^{[m_{\mathrm{R}}]}$ between the reference antenna and the n_{T}th (n_{R}th) antenna in the array depends on the chosen wavefront model, which can be planar if the sources are in the far-field [19], approximated spherical (Fresnel approximation [2]) or exactly spherical [4,8,9,20]. In this work, we adopt the exact spherical wavefront model given in equation (1) (for the receiving side) on the bottom of this page.

By stacking the matrices $\boldsymbol{Y}_p^{[m_{\mathrm{R}}]}$ with fixed m_{R} and varying p along the 3-mode, the data received at the m_{R}th array for P pulses can be represented as a three-dimensional tensor $\boldsymbol{\mathcal{Y}}_{(:,:,p)}^{\prime[m_{\mathrm{R}}]} = \boldsymbol{Y}_p^{[m_{\mathrm{R}}]} \in \mathbb{C}^{N_{\mathrm{R}} \times T}$. After permuting the first and the third indices in $\boldsymbol{\mathcal{Y}}^{\prime[m_{\mathrm{R}}]} \in \mathbb{C}^{N_{\mathrm{R}} \times T \times P}$, we can rewrite it as the tensor $\boldsymbol{\mathcal{Y}}^{[m_{\mathrm{R}}]} \in \mathbb{C}^{P \times T \times N_{\mathrm{R}}}$ (due to the page limitations, we refer the reader to [10] for detailed derivations) in the following way

$$\boldsymbol{\mathcal{Y}}^{[m_{\mathrm{R}}]} = \sum_{r=1}^{R} \alpha_r^{[m_{\mathrm{R}}]} \left(\boldsymbol{F}_r^{[m_{\mathrm{R}}]} \boldsymbol{C}_r^{\mathrm{T}}\right) \circ \boldsymbol{b}_r^{[m_{\mathrm{R}}]} + \boldsymbol{\mathcal{N}}^{[m_{\mathrm{R}}]} \in \mathbb{C}^{P \times T \times N_{\mathrm{R}}}, \tag{3}$$

where the columns of the matrix of reflection coefficients $\boldsymbol{F}_r^{[m_{\mathrm{R}}]} = \left[\, \boldsymbol{f}_r^{[m_R,1]}, \quad \ldots, \quad \boldsymbol{f}_r^{[m_R,M_T]} \,\right] \in \mathbb{C}^{P \times M_{\mathrm{T}}}$ are expressed as $\boldsymbol{f}_r^{[m_R,m_T]} = \left[\, \varrho_{r,1}^{[m_R,m_T]}, \quad \ldots, \quad \varrho_{r,P}^{[m_R,m_T]} \,\right]^{\mathrm{T}} \in \mathbb{C}^{P}$. Moreover, the matrix $\boldsymbol{C}_r = \left[\, \boldsymbol{c}_r^{[1]}, \quad \ldots, \quad \boldsymbol{c}_r^{[M_{\mathrm{T}}]} \,\right] \in \mathbb{C}^{T \times M_{\mathrm{T}}}$ is constructed from the vectors $\boldsymbol{c}_r^{[m_{\mathrm{T}}]} = \boldsymbol{S}^{[m_{\mathrm{T}}]} \boldsymbol{a}_r^{[m_{\mathrm{T}}]} \in \mathbb{C}^{T}$ that combine the transmitted signal and the transmit steering vectors. The representation of the data in (3) corresponds to the noise-corrupted coupled rank-$(L_r, L_r, 1)$ BTD [10,17,21] with the M_{R} tensors coupled in the 2-mode since the arrays receive the same transmitted data. We assume that the matrices $\boldsymbol{F}_r^{[m_{\mathrm{R}}]} \in \mathbb{C}^{P \times M_{\mathrm{T}}}$ and $\boldsymbol{C}_r \in \mathbb{C}^{T \times M_{\mathrm{T}}}$

$$\delta_{\mathrm{R},r,n_{\mathrm{R}}}^{[m_{\mathrm{R}}]} = \sqrt{\left(x_{\mathrm{R},r}^{[m_{\mathrm{R}}]} - x_{\mathrm{R},n_R}^{[m_{\mathrm{R}}]}\right)^2 + \left(y_{\mathrm{R},r}^{[m_{\mathrm{R}}]} - y_{\mathrm{R},n_R}^{[m_{\mathrm{R}}]}\right)^2 + \left(z_{\mathrm{R},r}^{[m_{\mathrm{R}}]} - z_{\mathrm{R},n_R}^{[m_{\mathrm{R}}]}\right)^2} - \rho_{\mathrm{R},r}^{[m_{\mathrm{R}}]}, \quad \forall n_{\mathrm{R}}, \forall m_{\mathrm{R}}. \tag{1}$$

in (3) have a full column rank equal to M_{T}, i.e., the number of pulses and snapshots is greater than M_{T}. In this case, the rank-$(L_r, L_r, 1)$ BTD is identifiable [22], and the matrices in (3) can be estimated through the coupled rank-$(L_r, L_r, 1)$ decomposition. Then, the final target parameter estimates are obtained via the solution of a system of linear equations and further processing, which we cover in the following.

3. COUPLED BTD-BASED TARGET LOCALIZATION

This section describes the main steps of the proposed COBRAS algorithm that utilizes the coupled rank-$(L_r, L_r, 1)$ decomposition for target localization in multi-static near-field radar systems. It includes the estimation of the initial decomposition of the received data, phase unwrapping, the solution of the system of linear equations, and the parameter extraction to calculate the final estimates.

3.1. Tensor decomposition and phase unwrapping

The first step of the algorithm is an estimation of the matrices $\boldsymbol{F}_r^{[m_{\mathrm{R}}]}$, $\boldsymbol{C}_r$, and the vectors $\boldsymbol{b}_r^{[m_{\mathrm{R}}]}$ which can be performed via an approximate coupled rank-$(L_r, L_r, 1)$ decomposition of the tensors $\boldsymbol{\mathcal{Y}}^{[m_{\mathrm{R}}]}$ with the block-rank R and the L_r-ranks equal to M_{T}. Several authors have proposed algorithms to compute the coupled rank-$(L_r, L_r, 1)$ decomposition, for example, the coupled SECSI-BTD algorithm that we propose in [17], structured data fusion algorithms in [23], or simultaneous diagonalization (SD) methods in [21,23,24]. In this study, we focus on the solution from [17] and compare its performance to the other schemes.

At this point, we should mention the additional matrix product ambiguity that occurs in the rank-$(L_r, L_r, 1)$ decompositions when estimating the product $\left(\boldsymbol{F}_r^{[m_{\mathrm{R}}]}\boldsymbol{C}_r^{\mathrm{T}}\right)$ as shown in [22]. Since the ambiguities in $\left(\boldsymbol{F}_r^{[m_{\mathrm{R}}]}\boldsymbol{C}_r^{\mathrm{T}}\right)$ are difficult to resolve, in this paper, we focus on the estimation of the steering vectors $\boldsymbol{b}_r^{[m_{\mathrm{R}}]}$ at the receive arrays, which are essentially unique (up to an arbitrary permutation and scaling) [21, 22] and can be used for the localization of the targets. We denote the estimated vectors $\boldsymbol{b}_r^{[m_{\mathrm{R}}]}$ as $\hat{\boldsymbol{b}}_r^{[m_{\mathrm{R}}]}$ and use them as columns in the matrices $\hat{\boldsymbol{B}}^{[m_{\mathrm{R}}]} = [\hat{\boldsymbol{b}}_1^{[m_{\mathrm{R}}]}, \ldots, \hat{\boldsymbol{b}}_R^{[m_{\mathrm{R}}]}] \in \mathbb{C}^{N_{\mathrm{R}} \times R}$. Based on the knowledge that at the reference (first) antenna, the path difference is equal to zero, the BTD scaling ambiguity can be corrected by dividing the vectors $\hat{\boldsymbol{b}}_r^{[m_{\mathrm{R}}]}$ by their first element.

As described in [8], to acquire the correct phases of the steering vectors $\hat{\boldsymbol{b}}_r^{[m_{\mathrm{R}}]}$, the unwrapping procedure has to be performed on the extracted phase angles as $\hat{\boldsymbol{\delta}}_r^{[m_{\mathrm{R}}]} = \frac{\lambda}{2\pi} \cdot \mathcal{U}\left\{\angle \hat{\boldsymbol{b}}_r^{[m_{\mathrm{R}}]}\right\}, \forall r$, where $\hat{\boldsymbol{\delta}}_r^{[m_{\mathrm{R}}]}$ is the vector of path difference estimates and $\mathcal{U}\{\bullet\}$ denotes the unwrapping algorithm. For uniformly distributed geometries, such as Uniform Linear Arrays (ULAs) or URAs, the correct phase unwrapping is possible if the element spacing is not larger than $\lambda/2$ with a simple 1-dimensional unwrapping algorithm [25] (in case of a URA it should be applied row- and column-wise). For other types of array geometries, 2- (or 3-) dimensional unwrapping algorithms should be applied [8, 26].

3.2. Solving the system of linear equations

In order to calculate the target location parameters, the following post-processing steps are applied independently for every $\hat{\boldsymbol{\delta}}_r^{[m_{\mathrm{R}}]}, \forall r$, $\forall m_{\mathrm{R}}$. Since the processing steps are the same for every receiving array, for notational simplicity, we drop the superscript $[m_{\mathrm{R}}]$ and the subscript R, denoting the array number and the receive side, respectively. Substituting the estimated path difference $\hat{\delta}_{r,n_{\mathrm{R}}}$ into (1), moving ρ_r to the left side, and taking the square results in

$$\left(\hat{\delta}_{r,n_{\mathrm{R}}} + \rho_r\right)^2 = \left(x_r - x_{n_{\mathrm{R}}}\right)^2 + \left(y_r - y_{n_{\mathrm{R}}}\right)^2 + \left(z_r - z_{n_{\mathrm{R}}}\right)^2 . \tag{4}$$

By expanding (4) further, we get

$$\hat{\delta}_{r,n_{\mathrm{R}}}^2 + 2\rho_r\hat{\delta}_{r,n_{\mathrm{R}}} + \rho_r^2 = \underbrace{x_r^2 + y_r^2 + z_r^2}_{\rho_r^2} + \underbrace{x_{n_{\mathrm{R}}}^2 + y_{n_{\mathrm{R}}}^2 + z_{n_{\mathrm{R}}}^2}_{d_{n_{\mathrm{R}}}^2} - 2\left(x_r x_{n_{\mathrm{R}}} + y_r y_{n_{\mathrm{R}}} + z_r z_{n_{\mathrm{R}}}\right). \tag{5}$$

which results in a set of $N_{\mathrm{R}} - 1$ linear equations (since the reference antennas are located at the origin of the system of coordinates, $x_1 = y_1 = z_1 = 0$, and $\hat{\delta}_{r,1} = 0, \forall r$) [8]

$$2\underbrace{\begin{bmatrix} x_2 & y_2 & z_2 & \hat{\delta}_{r,2} \\ x_3 & y_3 & z_3 & \hat{\delta}_{r,3} \\ \vdots & \vdots & \vdots & \vdots \\ x_{N_{\mathrm{R}}-1} & y_{N_{\mathrm{R}}-1} & z_{N_{\mathrm{R}}-1} & \hat{\delta}_{r,N_{\mathrm{R}}-1} \end{bmatrix}}_{\boldsymbol{X}_r \in \mathbb{R}^{(N_{\mathrm{R}}-1)\times 4}} \boldsymbol{p}_r = \underbrace{\begin{bmatrix} d_2^2 - \hat{\delta}_{r,2}^2 \\ d_3^2 - \hat{\delta}_{r,3}^2 \\ \vdots \\ d_{N_{\mathrm{R}}-1}^2 - \hat{\delta}_{r,N_{\mathrm{R}}-1}^2 \end{bmatrix}}_{\boldsymbol{y}_r \in \mathbb{R}^{(N_{\mathrm{R}}-1)\times 1}} \tag{6}$$

where $d_{n_{\mathrm{R}}}^2 = x_{n_{\mathrm{R}}}^2 + y_{n_{\mathrm{R}}}^2 + z_{n_{\mathrm{R}}}^2$ is the distance from the reference antenna (located at the origin) to the n_{R}th antenna, and

$$\boldsymbol{p}_r = \begin{bmatrix} x_r \\ y_r \\ z_r \\ \sqrt{x_r^2 + y_r^2 + z_r^2} \end{bmatrix} = \begin{bmatrix} \rho_r \cos(\phi_r)\cos(\theta_r) \\ \rho_r \sin(\phi_r)\cos(\theta_r) \\ \rho_r \sin(\theta_r) \\ \rho_r \end{bmatrix} . \tag{7}$$

The set of equations in (6) allows estimating the location of targets in the full 3D space around the receive array if the antenna array geometry exhibits diversity in all spatial directions (i.e., the arrays are not planar). In the case of planar antenna arrays, for example, URAs, the matrix $\boldsymbol{X}_r$ in (6) will not have full column rank. In such a situation, we choose a local system of coordinates with the origin at the reference antenna such that all antennas lie in the x-y-plane. Then, $z_{n_{\mathrm{R}}} = 0$, $\forall n_{\mathrm{R}}$ and the parameter vector $\boldsymbol{p}_r$ reduces to (7) without the third row. Consequently, the matrix $\boldsymbol{X}_r$ in (6) is transformed into a matrix of size $(N_{\mathrm{R}} - 1) \times 3$ ($\boldsymbol{X}_r$ in (6) without the third column). In this case, the parameter estimation is only possible in the upper half of the 3D space where $z_r > 0$ (or $0 \leq \theta_r \leq \pi/2$).

The solution vector can, for example, be found by means of least squares (LS) or total least squares (TLS) [27].

3.3. Parameter extraction

In the general 3D case, the final range, azimuth, and elevation estimates can be computed as

$$\rho_r = \left(\hat{\boldsymbol{p}}_r\right)_{(4)}, \quad \phi_r = \operatorname{atan2}\left(\frac{\left(\hat{\boldsymbol{p}}_r\right)_{(2)}}{\rho_r}, \frac{\left(\hat{\boldsymbol{p}}_r\right)_{(1)}}{\rho_r}\right), \tag{8a}$$

$$\theta_r = \operatorname{atan2}\left(\frac{\left(\hat{\boldsymbol{p}}_r\right)_{(3)}}{\rho_r}, \frac{\sqrt{\left(\hat{\boldsymbol{p}}_r\right)_{(1)}^2 + \left(\hat{\boldsymbol{p}}_r\right)_{(2)}^2}}{\rho_r}\right), \tag{8b}$$

where $\operatorname{atan2}(y, x)$ denotes the four quadrant arctangent function and $(\boldsymbol{a})_{(i)}$ denotes the ith element of $\boldsymbol{a}$.

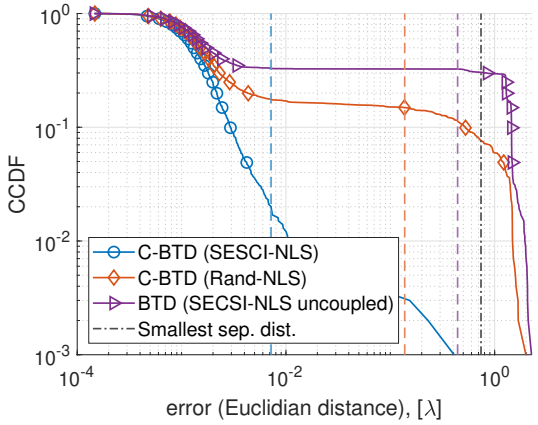

Fig. 2: CCDF vs. errors in terms of the Euclidian distance between true and estimated locations. $\mathrm{SNR} = 30\,\mathrm{dB}$. 1000 Monte-Carlo trials.

If all the array antennas are in the same plane (e.g., URA case), the range is $\rho_r = (\hat{\boldsymbol{p}}_r)_{(3)}$ and the elevation is computed as

$$\theta_r = \cos^{-1}\left(\frac{\sqrt{(\hat{\boldsymbol{p}}_r)^2_{(1)} + (\hat{\boldsymbol{p}}_r)^2_{(2)}}}{\rho_r}\right). \tag{9}$$

The equation (9) additionally provides a simple reliability test that can be applied in this case. If the value of $\sqrt{(\hat{\boldsymbol{p}}_h)^2_{(1)} + (\hat{\boldsymbol{p}}_h)^2_{(2)}}/\rho_h$ is larger than one, then the test has failed, and the location estimates should be considered as not reliable.

4. SIMULATION RESULTS

This section presents the empirical validation of the COBRAS algorithm, demonstrating its performance and the impact of the different rank-$(L_r, L_r, 1)$ decomposition algorithms on the localization accuracy.

For the simulations, we consider a multi-static MIMO radar system with $M_\mathrm{T} = 3$ transmitting arrays and $M_\mathrm{R} = 2$ receiving arrays. The carrier frequency is $f_c = 50\,\mathrm{GHz}$ which results in a wavelength of $\lambda = c/f_c \approx 0.6$ cm. As the transmitting and receiving arrays, we use URAs of 10×10 elements, resulting in $N_\mathrm{T} = N_\mathrm{R} = 100$. The antenna element spacing is set to $\lambda/2$. The Cartesian coordinates of the reference transmit antennas are $\{0, 0, 0\}$, $\{0, 12\lambda, 0\}$, and $\{0, 24\lambda, 0\}$, and the coordinates of the receiving reference antennas are $\{16\lambda, 0, 0\}$, $\{16\lambda, 17\lambda, 0\}$. The antenna arrays are rotated about the y-axis by the angles $\gamma_\mathrm{T} = 140^\circ$ and $\gamma_\mathrm{R} = 30^\circ$, for the transmit and receive sides, respectively. The number of time snapshots is set to $T = 200$, and the number of pulses is $P = 100$. The size of the received data tensors $\boldsymbol{\mathcal{Y}}^{[1]}$ and $\boldsymbol{\mathcal{Y}}^{[2]}$ is then $100\times200\times100$. The range, azimuth, and elevation parameters of the $R = 3$ closely spaced targets with respect to the reference antennas of two receive arrays are $\boldsymbol{\Theta}^{[1]}_{R,1} = \{22\lambda, 116.6^\circ, 44.7^\circ\}$, $\boldsymbol{\Theta}^{[1]}_{R,2} = \{21\lambda, 112.9^\circ, 45.7^\circ\}$, $\boldsymbol{\Theta}^{[1]}_{R,3} = \{23.4\lambda, 110.6^\circ, 43.1^\circ\}$, $\boldsymbol{\Theta}^{[2]}_{R,1} = \{17.9\lambda, -156.8^\circ, 63.8^\circ\}$, $\boldsymbol{\Theta}^{[2]}_{R,2} = \{16.4\lambda, -148.4^\circ, 66^\circ\}$, and $\boldsymbol{\Theta}^{[2]}_{R,3} = \{17.1\lambda, -170.5^\circ, 69.1^\circ\}$, respectively. The example scenario used for the simulations is illustrated in Fig. 1. The reflection coefficients and the transmitted signal after matched-filtering at the receiver are drawn from a zero mean complex Gaussian distribution with unit variance. The additive noise tensor $\boldsymbol{\mathcal{N}}^{[m_\mathrm{R}]}$ is modeled as an i.i.d. zero mean spatially and temporally white additive noise with variance σ_n^2. The simulations were performed for $K = 1000$ trials.

We evaluate the accuracy of the target localization, defining the errors in terms of the Euclidean distance between the true ($\boldsymbol{u}_r$) and the estimated ($\hat{\boldsymbol{u}}_{r,k}$) location of the target as

$$\mathrm{err} = \sqrt{\eta(\hat{\boldsymbol{u}}_{r,k})\,\|\boldsymbol{u}_r - \hat{\boldsymbol{u}}_{k,r}\|^2} \quad \forall r, \forall k, \tag{10}$$

where $k \in 1, \ldots, K$ is a trial index and the

$$\eta(\hat{\boldsymbol{u}}) = \begin{cases} 1, & \text{if } \hat{\boldsymbol{u}} \text{ passed the reliability test} \\ 0, & \text{otherwise} \end{cases} \tag{11}$$

represents the indicator function of the reliability test described at the end of Section 3.3. Therefore, only the trials in which the reliability test did not fail are taken into account.

The complementary cumulative distribution function (CCDF) of the errors in terms of the Euclidian distance for the $\mathrm{SNR} = 30\,\mathrm{dB}$ is shown in Fig. 2 (these are the results for the second array averaged among all targets; for the first array, the results are similar). The colored vertical lines in the plots represent the mean values for each curve. The dash-dotted line denotes the minimum separation distance between targets [9]. We compare three BTD algorithms for the estimation of the steering matrices (the other steps are performed according to COBRAS): (i) coupled rank-$(L_r, L_r, 1)$ BTD algorithm from [17] (nonlinear least squares (NLS) with SECSI-based initialization, blue curve); (ii) NLS solution for coupled rank-$(L_r, L_r, 1)$ BTD from [28] (random initialization, orange curve); and (iii) non-coupled solution from [29] (purple curve). In the third case, only the data from one given array is processed. Therefore, there is no joint processing, and the coupling is not considered. As can be observed, the SECSI-NLS scheme outperforms the considered alternatives, especially the non-coupled approaches. This can be explained by the more reliable initialization provided by the SECSI algorithm, which reduces the number of outliers. Conversely, the NLS solution with random initialization does not always converge. The inferior performance of the single BTD demonstrates the benefits of the coupling: the localization is more accurate and reliable when data from both arrays is processed jointly.

The estimation performances can be further improved by, for example, constructing the system in (6) using the estimates from both arrays and using a weighted least squares solution. Another solution is to consider only the estimates from the array that passed the reliability test in (11) or take into account only the estimates from the array that is located closer to the target.

5. CONCLUSIONS

This paper presented a high-resolution coupled rank-$(L_r, L_r, 1)$ decomposition-based near-field localization algorithm for multi-static MIMO radar systems. The COBRAS algorithm performs the target location parameters estimation in 3D space based on the exact wavefront model and is applicable to arbitrary array geometries. Compared to the far-field planar wavefront, the use of the exact wavefront model enables the estimation of not only the direction-of-arrival parameters but also the range and, consequently, the position of the target. Moreover, the use of massive antenna arrays increases the Fresnel region and makes the near-field assumption applicable in practical scenarios. Furthermore, the algorithm utilizes a reliability measure, which allows discarding unreliable parameter estimates. The simulation results show that the employment of coupling and joint processing of the data from multiple arrays improves the localization performance compared to the non-coupled solutions.

6. REFERENCES

[1] M. Cui, Z. Wu, Y. Lu, X. Wei, and L. Dai, "Near-Field MIMO Communications for 6G: Fundamentals, Challenges, Potentials, and Future Directions," *IEEE Communications Magazine*, vol. 61, no. 1, pp. 40–46, 2023.

[2] M. Haardt, R. N. Challa, and S. Shamsunder, "Improved bearing and range estimation via high-order subspace based Unitary ESPRIT," in *Proc. 30th Asilomar Conf. Signals, Systems and Computers*, Pacific Grove, CA, USA, Nov. 1996, pp. 380–384.

[3] M. N. El Korso and M. Pesavento, "Performance analysis for near field source localization," in *Proc. IEEE 7th Sensor Array and Multichannel Signal Processing Workshop (SAM)*, 2012, pp. 197–200.

[4] P. R. Singh, Y. Wang, and P. Chargé, "Bistatic MIMO radar for near field source localisation using PARAFAC," *Electronics Letters*, vol. 52, no. 12, pp. 1060–1061, Apr. 2016.

[5] E. Zhou, H. Jiang, and H. Qi, "4-D parameter estimation in bistatic MIMO radar for near-field target localization," in *Proc. IEEE Int. Wireless Symp.*, Shenzhen, China, Mar. 2015.

[6] W. Zuo, J. Xin, H. Ohmori, N. Zheng, and A. Sano, "Subspace-Based Algorithms for Localization and Tracking of Multiple Near-Field Sources," *IEEE Journal of Selected Topics in Signal Processing*, vol. 13, pp. 156–171, Mar. 2019.

[7] P. R. Singh, Y. Wang, and P. Chargé, "Near field targets localization using bistatic MIMO system with spherical wavefront based model," in *Proc. 25th European Signal Processing Conf. (EUSIPCO)*, Kos, Greece, Aug. 2017, pp. 2408–2412.

[8] I. Podkurkov, L. Hamidullina, E. Traikov, M. Haardt, and A. Nadeev, "Tensor-Based Near-Field Localization in Bistatic MIMO Radar Systems," in *Proc. 22nd International ITG Workshop on Smart Antennas (WSA 2018)*, 2018, pp. 1–8.

[9] I. Podkurkov, G. Seidl, L. Khamidullina, A. Nadeev, and M. Haardt, "Tensor-Based Near-Field Localization Using Massive Antenna Arrays," *IEEE Transactions on Signal Processing*, vol. 69, pp. 5830–5845, 2021.

[10] J.-X. Yang, X.-F. Gong, H. Li, Y.-G. Xu, and Z.-W. Liu, "Using Coupled Multilinear Rank-$(L, L, 1)$ Block Term Decomposition in Multi-Static-Multi-Pulse MIMO Radar to Localize Targets," in *Proc. Advances in Neural Networks – ISNN 2019*. 2019, pp. 565–574, Springer International Publishing.

[11] G. Chen, Z.-F. Zhu, J.-X. Yang, and X.-F. Gong, "Multi-target Localization with MIMO Radar via Coupled Canonical Polyadic Decomposition," in *Proc. IEEE International Conference on Signal, Information and Data Processing (ICSIDP)*, 2019.

[12] N. Sidiropoulos, R. Bro, and G. Giannakis, "Parallel factor analysis in sensor array processing," *IEEE Transactions on Signal Processing*, vol. 48, no. 8, pp. 2377–2388, Aug. 2000.

[13] M. Sørensen, I. Domanov, and L. De Lathauwer, "Coupled Canonical Polyadic Decompositions and Multiple Shift Invariance in Array Processing," *IEEE Transactions on Signal Processing*, vol. 66, no. 14, pp. 3665–3680, July 2018.

[14] Z. Lin, T. Lv, W. Ni, J. A. Zhang, and R. P. Liu, "Tensor-Based Multi-Dimensional Wideband Channel Estimation for mmWave Hybrid Cylindrical Arrays," *IEEE Transactions on Communications*, vol. 68, no. 12, pp. 7608–7622, Dec. 2020.

[15] H. Zheng, C. Zhou, Z. Shi, Y. Gu, and Y. D. Zhang, "Coarray Tensor Direction-of-Arrival Estimation," *IEEE Transactions on Signal Processing*, vol. 71, pp. 1128–1142, 2023.

[16] H. Chen, F. Ahmad, S. Vorobyov, and F. Porikli, "Tensor Decompositions in Wireless Communications and MIMO Radar," *IEEE Journal of Selected Topics in Signal Processing*, vol. 15, no. 3, pp. 438–453, 2021.

[17] I. Safiullin, L. Khamidullina, A. A. Korobkov, and M. Haardt, "Enhanced Computation of the Coupled Block-Term Decomposition in Multilinear Rank Terms," in *Proc. IEEE 12th Sensor Array and Multichannel Signal Processing Workshop (SAM)*, Trondheim, Norway, June 2022, pp. 400–404.

[18] M. Richards, W. Holm, and J. Scheer, *Principles of Modern Radar: Basic Principles*, Electromagnetics and Radar. Institution of Engineering and Technology, 2010.

[19] P. Stoica and A. Nehorai, "MUSIC, maximum likelihood, and Cramer-Rao bound," *IEEE Transactions on Acoustics, Speech, and Signal Processing*, vol. 37, no. 5, pp. 720–741, May 1989.

[20] L. Khamidullina, I. Podkurkov, and M. Haardt, "Conditional and Unconditional Cramér-Rao Bounds for Near-Field Localization in Bistatic MIMO Radar Systems," *IEEE Transactions on Signal Processing*, vol. 69, pp. 3220–3234, 2021.

[21] M. Sørensen and L. De Lathauwer, "Coupled Canonical Polyadic Decompositions and (Coupled) Decompositions in Multilinear Rank-$(L_{r,n}, L_{r,n}, 1)$ Terms—Part I: Uniqueness," *SIAM Journal on Matrix Analysis and Applications*, vol. 36, pp. 496–522, 04 2015.

[22] L. De Lathauwer, "Decompositions of a Higher-Order Tensor in Block Terms—Part II: Definitions and Uniqueness," *SIAM Journal on Matrix Analysis and Applications*, vol. 30, no. 3, pp. 1033–1066, 2008.

[23] L. Sorber, M. Van Barel, and L. De Lathauwer, "Structured Data Fusion," *IEEE Journal of Selected Topics in Signal Processing*, vol. 9, no. 4, pp. 586–600, 2015.

[24] M. Sørensen, I. Domanov, and L. De Lathauwer, "Coupled Canonical Polyadic Decompositions and (Coupled) Decompositions in Multilinear Rank-$(L_{r,n}, L_{r,n}, 1)$ Terms—Part II: Algorithms," *SIAM Journal on Matrix Analysis and Applications*, vol. 36, pp. 1015–1045, Jan. 2015.

[25] K. Itoh, "Analysis of the phase unwrapping problem," *Applied Optics*, vol. 21, no. 14, pp. 2470, July 1982.

[26] D. C. Ghiglia and M. D. Pritt, *Two-Dimensional Phase Unwrapping: Theory, Algorithms, and Software*, vol. 4, Wiley New York, 1998.

[27] G. H. Golub and C. F. Van Loan, *Matrix Computations*, The Johns Hopkins University Press, fourth edition, 2013.

[28] N. Vervliet, O. Debals, L. Sorber, M. van Barel, and L. De Lathauwer, "Tensorlab 3.0," Mar. 2016.

[29] L. Khamidullina, G. Seidl, I. A. Podkurkov, A. A. Korobkov, and M. Haardt, "Enhanced Solutions for the Block-Term Decomposition in Rank-$(L_r, L_r, 1)$ Terms," *IEEE Transactions on Signal Processing*, vol. 71, pp. 2608–2621, 2023.